Nanoscale

Accepted Manuscript

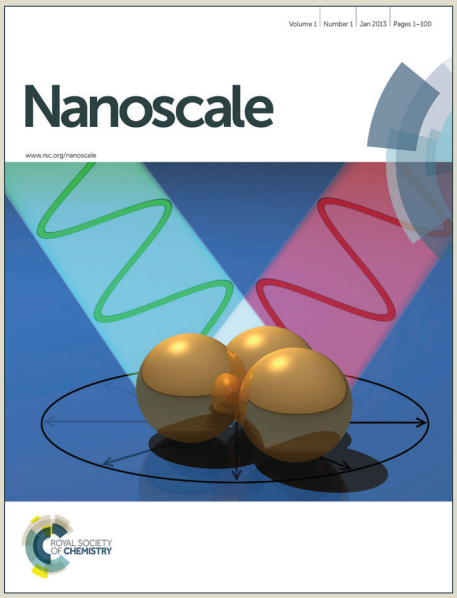

Running title: Distribution and toxicity of IOMNs in mice

Size Dependent Biodistribution and Toxicokinetics of Iron Oxide Magnetic Nanoparticles in Mice

Lin Yang[1, 2#], Huijuan Kuang[1#], Wanyi Zhang[1, 3#], Zoraida P. Aguilar[4], Yonghua Xiong[2], Weihua Lai[1], Hengyi Xu[1] and Hua Wei[2]**

Co-first authors.

[1]State Key Laboratory of Food Science and Technology, Nanchang University, Nanchang 330047, China

[2]Jiangxi-OAI Joint Research Institute, Nanchang University, Nanchang 330047, China

[3] The Second Affiliated Hospital of Nanchang University, Nanchang 330000, China

[4] Zystein, LLC., Fayetteville, AR 72704, USA

*Correspondence to:

Dr. Hengyi Xu, State Key Laboratory of Food Science and Technology, Nanchang University. Address: 235 Nanjing East Road, Nanchang 330047, P.R. China.

Phone: +0086-791-8830-4447-ext-9512. Fax: +0086-791-8830-4400.

E-mail: kidyxu@163.com; HengyiXu@ncu.edu.cn.

Dr. Hua Wei, Jiangxi-OAI Joint Research Institute, Nanchang University.

Address: 235 Nanjing Donglu, Nanchang 330047, P.R. China.

Phone: +86-791-8833-4578, Fax: +86-791-8833-3708. E-mail: weihua114@live.cn.

Abstract

In spite of the immense benefits from iron oxide magnetic nanoparticles (IOMNs), there is scanty information regarding its metabolic activities and toxicity *in vivo*. In this study, we investigated the size dependent *in vivo* biodistribution, toxicokinetics, and toxicity and gene expression changes of various sizes of carboxyl coated IOMNs (diameters of 10, 20, 30, and 40 nm). Our findings demonstrated that the various sizes of IOMNs accumulated primarily in the liver and spleen on the first day post-injection, Interestingly, size dependent biodistribution and transport were observed: the smallest IOMNs (10 nm) showed the highest uptake by the liver, whereas the largest IOMNs (40 nm) showed the highest uptake by the spleen. Moreover, the IOMNs with the smallest size (10 nm) were cleared faster from the liver and kidney, but more readily entered the brain and the uterus. IOMNs with the largest size (40 nm) accumulated more readily but were easily eliminated in the spleen. However, the level of iron in heart decreased in all IOMNs exposed group. In addition, blood biochemistry, hematological analyses and histological examination demonstrated that there was no apparent acute toxicity caused by IOMNs in mice. However, smaller IOMNs (10 nm and 20 nm) more effectively changed the expression level of sensitive genes related to oxidant stress, iron transport, metabolic process, apoptosis, and others.

Key words: iron oxide magnetic nanoparticles, size dependent biodistribution, magnetic resonance imaging (MRI), toxicokinetics, gene expression

Introduction

Iron oxide magnetic nanoparticles (IOMNs) hold great potential in a wide variety of biomedical and biological applications such as contrast enhancement of magnetic resonance imaging (MRI), targeted drug or gene delivery, tissue engineering, detoxification of biological fluids, hyperthermia in cancer therapy, cell labeling, cell sorting and immunoassay, etc.[1-4] It is currently the most popular superparamagnetic material used *in vivo*, with several commercialized products used as contrast agents or at different stages of clinical trials.[1,5,6] Similar to other nanoparticles (NPs), IOMNs possess unique physicochemical characteristics such as nanoscale size, quantum size effects, and large surface area to mass ratio.[7] Moreover, IOMNs show excellent chemical stability, thermal and magnetic properties that promote innovative applications, such as *in vivo* dual imaging (T2-weighted magnetic resonance images and optical fluorescence images).[8] IOMNs have been most visible in the mononuclear phagocyte system (MPS) including the liver, spleen, lymph nodes and bone marrow *in vivo* applications.[1] However, due to the high particle reactivity and small size, IOMNs have been shown to be toxic to cells, tissues and organs, and organisms as compared with the bulk sized particles of the same composition based on accumulated experimental data.[9-14]

Many *in vitro* articles have investigated the cytotoxicity of IOMNs and found inconsistent results.[6,15-21] Previous studies demonstrated that IOMNs induced alterations in cell behavior, morphology, and viability, as well as induced cellular oxidative stress and genotoxicity.[16,17,20] Whereas some other researchers found that

IOMNs (Ferumoxtran-10) was non-toxic to cells (no induction of cytokine and superoxide anions production, no disturbance of Fc-receptor-mediated phagocytosis) even at high concentration (10 mg/mL) and when they were retained in lysosomes of cells for extended periods of time.[18,19] Although results from these *in vitro* cytotoxicity tests varied, they can still provide meaningful insights for the evaluation of possible side effects of IOMNs *in vivo*.[15] However, there is limited number of articles that showed *in vivo* assessment of toxicokinetic processes such as biodistribution, degradation, elimination, and toxicity profile of IOMNs that also looked into possible subtle changes such as genotoxicity that led to observed toxicity in the *in vitro* studies.

In recent years, few toxicological studies reported the toxicokinetic parameters, tissue distribution, and gene expression changes of IOMNs in mice or rats after various routes of exposure.[5,6,22-25] Researchers found systemic accumulation and retention of Fe_2O_3 NPs in rat lungs following intra-tracheal infusion.[26] Another group studied the distribution, short-term toxicity, animal survival, serum biochemistry, oxidative stress, and organ histology of IOMNs in rats following intravenous injection. The IOMNs accumulated locally in the liver, spleen, brain, heart, lung, and kidney and did not cause any considerable toxicity *in vivo*.[22] In addition, it was demonstrated that Fe_3O_4 NPs exhibited considerably higher systemic toxicity than the microparticle forms.[24]

The hydrodynamic size of IOMNs affects the magnetic and biological properties, the biodistribution, toxicokinetics, elimination, and toxicity which are closely related to

the synthesis methodology, surface characteristics, as well as particle size.[1,7,27-31] Along these lines, it has been reported that the distribution of gold NPs in mice was size dependent such that small sized particles (5 and 10 nm) mainly accumulated in the liver; medium sized particles (30 nm) were stored in the spleen, whereas the larger particles (60 nm) were not observed in these organs.[14] Nanoparticles such as InAs/ZnS QDs coated with short polyethylene glycol (PEG) chain (< 5.5 nm diameter) showed rapid uptake in the liver and were easily cleared by the kidneys, whereas larger QDs (> 6.5 nm diameter) were accumulated in the lymph nodes, pancreas and the intestines; these were more likely subject to hepatic clearance.[28] Moreover, PEG-coated magnetite NPs showed the doubled residence time than meso-2,3-dimercaptosuccinic acid (DMSA) coated NPs in blood.[32] In addition, *in vivo* studies on large IOMNs showed shorter blood residence time and were likely cleared by the macrophages in the liver and spleen. In contrast, smaller IOMNs showed a longer blood half-life and were mainly stored in the macrophages of the lymph nodes or peripheral tissue.[19,33] Thus, the diameter of IOMNs may play an important role in its kinetic behavior *in vivo* but there are few studies had explored the size effects on their distribution, transportation, elimination, acute toxicity and genotoxicity profile. Moreover, IOMNs that are coated with amphiphilic polymers with reactive carboxyl group (carboxyl-coated IOMNs) can be used for *in vivo* tumor imaging and *in vitro* cancer cell separation after conjugation with antibody, peptide, and other amine containing molecules.[3,34] Thus, we evaluated carboxyl-coated IOMNs *in vivo* with the purpose of systematically assessing their size dependent (10, 20, 30, 40 nm IOMNs)

biodistribution, toxicokinetics, acute toxicity, and gene expression changes in mice to provide valuable information and possible insights for understanding future use in nanomedicine.

Experimental section

Materials

Iron oxide (Fe_3O_4) magnetic NPs with different sizes (10, 20, 30, and 40 nm diameter) used in this experiment came from Ocean NanoTech, LLC (San Diego, CA). Hydrophobic IOMNs were prepared using iron oxide powder as the iron precursor, oleic acid as the ligands, and octadecene as the solvent. To convert the IOMNs into biocompatible nanoparticles, these were coated with amphiphilic polymers containing carboxylic acid as functional groups as reported previously.[3] The sizes of the IOMNs were confirmed with transmission electron microscopy (TEM) prior to performance of following experiments (Fig. 1a, b, c, d). Briefly, samples were prepared by dropping solution of IOMNs onto an agar carbon-coated copper grid (400 meshes) and the solvent was evaporated, TEM images were obtained at 50-100 K magnifications with a JEOL transmission electron microscope (JEOL USA, Inc. Peabody, MA) operating at 100 kV as previously described.[3] The hydrodynamic size distributions of IOMNs (n=4) (Fig. 1e) were measured by dynamic light scattering (DLS) using a Zetatrac Ultra 151 (Microtrac Inc., Montgomeryville, PA). To determine the average surface charge on the IOMNs, the zeta potential was also established using the Zetatrac Ultra 151.

Animal studies

Sixty adult female KunMing mice (30-35 g each) were purchased from the experimental animal center of Nanchang University, China. The animals were raised in an animal facility at 25°C with a 12 h light/dark cycle; the animals were supplemented with food and water *ad libitum*. All procedures involving animals were approved by the Animal Care Review Committee (approval number 0064257), Nanchang University, Jiangxi, China and care for institutional animal care committee guidelines. To compare the size dependent toxicity, four kinds of IOMNs with different diameters were diluted using ultrapure water resulting in the same mass concentration of 3 mg/mL. Two consecutive tail-vein injections (injected at 0 h and 24 h) of 0.1 mL IOMNs (approximate 20 mg/kg in total) solutions were administered to mice using a dose that was at medium level compared to in recent studies,[23,33] which was about eight times higher than the doses that were used for clinical imaging.[22] The weight of the mice, food intake, and physiological behaviors were examined every day. The mice were randomly divided into five groups (twelve in each group, four IOMNs treatment groups corresponding with the sizes of the nanoparticles and one control group treated with physiological saline) and were sacrificed at two time points: 1 day and 7 day post injection (n=6). Sample collections of feces were scheduled at three time points: 1 day, 3 day, and 7 day post injection.

Biodistribution and toxicokinetics analysis

Atomic absorption spectroscopy (AAS, model iCE 3500, Thermo Scientific, San Jose, CA) was used to determine the iron (Fe) contents in the organs. The animals were

sacrificed at day 1 and day 7 post IOMNs injection. Samples of the liver were isolated and a small portion of tissue was immediately frozen in liquid nitrogen and stored at -80 ^{o}C for total RNA extraction. Other organs (liver, spleen, kidneys, heart, lungs, brain, intestine, stomach, and uterus) were carefully collected, washed twice in physiological saline to remove the residual blood in the organs, and weighed for visceral index measurement. A small fraction of each organ (liver, spleen, and kidney) was isolated and fixed in 10% paraformaldehyde. The remaining portion of each organ (0.1-0.5 g) except a portion of the liver were dissolved in 12 mL digestion solution (HNO_3:$HClO_4$=5:1) and were heated to 230°C. The temperature was increased to 280°C when the reaction reached equilibrium. The digested organ samples were diluted with ultrapure water to 25 mL after removal from the heating block. The diluted organ sample digests were used to determine the iron concentrations with AAS.

Blood biochemistry and hematology

Blood samples were harvested from the five mice groups at day 1 and day 7 after injection of 20 mg IOMNs/kg body weight (n=6). Briefly, blood collected from orbital sinus by quickly removing the eyeball, and a small amount of whole blood (0.3-0.4 mL, potassium EDTA collection tube) was used for hematology analysis, and approximately 0.8 mL blood was centrifuged to obtain at least 0.25 mL blood plasma for serum biochemistry. The residual blood from each mouse was exhausted from the

eye socket. The whole blood was treated with anticoagulant and the blood serum was examined at the First Affiliated Hospital of Nanchang University, Nanchang, China.

Pathological examinations

The mice were sacrificed after blood collection and the organs (liver, spleen, and kidneys) were harvested and a small portion of each organ was fixed in 10% paraformaldehyde. Subsequently, isolated tissues were embedded in paraffin blocks (previously melted at 58°C) and frozen at 4°C before 3-5 μm sections were cut and stained with hematoxylin and eosin (H&E) for histological examination. The stained slices were observed under an Olympus optical microscope (Tokyo, Japan).

RT-qPCR analysis

Among all the organs collected from each group of animals, the liver showed high accumulation of iron. Thus, the liver was selected to determine possible changes in gene expressions. Total RNA was isolated using Takara MiniBEST Universial RNA extraction Kit (code no. 9767) according to the manufacturer's protocol. cDNA was synthesized using Thermo scientific RevertAid First stand cDNA synthesis kit (#6162, #k1622) with total RNA (480 ng) following measured the concentration of total RNA using NanoDrop 1000 spectrophotometer (Thermo scientific Inc.) and examined by agarose gel electrophoresis (data not shown). The qPCR primers were synthesized by Invitrogen China (Shanghai, China), and are listed in the supplemented Tab. S1. The

gene encoding glyceraldehyde-3-phosphate dehydrogenase (*GADPH*) was used as housekeeping gene. Quantitative PCR was performed using SYBR® *Premix Ex Taq*™ II (TakaRa Code: DRR820A). The reaction mixture was prepared by mixing aliquots of cDNA, 0.8 μL (10 μM) each primer, 10 μL SYBR® *Premix Ex Taq*™ II (2×) and 0.4 μL ROX Reference Dye II (50×) in a final volume of 20 μL. Amplification was carried on a 7900HT Fast real-time System (Applied Biosystems, Foster city, CA) with the following two-step thermal cycling program: 1 cycle at 95°C for 1 min, then 40 cycles of 95°C for 5 s, then 60°C for 1 min. Relative gene expression levels was determined by the critical threshold (Ct) number and calculated using the $2^{-\Delta\Delta Ct}$ method,[35, 36] with *GADPH* utilized as reference gene for all test groups.

Statistical analysis

All the data were expressed as mean ± standard deviation (n=6). Comparison of results among the groups were carried out by one-way analysis of variance (ANOVA) and L.S.D. test[37] using SPSS v16.0 (SPSS, Inc., Chicago, IL); *: $p < 0.05$ was considered statistically significant when compared to the control; **$p<0.01$ was considered highly statistically significant when compared to the control.

Results and discussion

Characterization of IOMNs

To explore the effects of size of IOMNs *in vivo* in mice, four sizes of IOMNs with diameters of 10, 20, 30, and 40 nm were used in this study. As shown in Fig. 1a, b, c, and d, the four sizes of IOMNs exhibited uniform, spherical, and monodisperse state under the TEM. The DLS measured hydrodynamic size distributions of the IOMNs (shown in Fig.1e) were 14.32±3.48, 25.41±5.25, 34.30±6.43, and 43.10±8.15 nm (n=4) corresponding to the TEM measurements (supplemental Tab. S2**,** n=4). The DLS measurements depend on the core and the surface conditions that were subject to water of hydration when the IOMNs were dissolved in water or in aqueous buffer resulting in increased size compared with the TEM size measurements. Aside from determining the hydrodynamic sizes, the DLS instrument was also used to establish the average surface charge on the IOMNs by measuring the zeta potential. The results indicated that the IOMNs chosen for the studies had an overall negative zeta potential with -50.63±8.26 (10 nm), -43.75±8.09 (20 nm), -41.45±7.32 (30 nm), and -40.05±8.92 mV (40 nm), respectively. Additionally, electrophoretic mobility towards a positive pole was also determined using gel electrophoresis. The results (data not shown) indicated that all the IOMNs used in this study migrated towards the positive pole at size-dependent rates having the smallest travel the fastest and the biggest travelling the slowest.

Size dependent biodistribution and transportation

To harness the benefits of IOMNs in nanomedicine and biology,[1,4] it is necessary to understand the size dependent biodistribution, toxicokinetics and toxicity of IOMNs *in vivo*. Additionally, particle size plays an important role in magnetic properties, stability, blood half-life, biodistribution, uptake, and elimination of IOMNs.[12,22,28,33] In our studies, the sizes of IOMNs did not affect the daily animal body weight as shown in Fig.2 (n=6). There was also no effect on food intake and behavior of the animals. Furthermore, the various sizes did not show significant effect on the weight of various organs (lung, liver, spleen, heart, kidney, and brain) in comparison with the control (see supplemental Tab. S3**,** n=6).

The distribution and toxicokinetics of IOMNs were directly related with the iron content in the various organs that was established using AAS. As shown in Tab. 1 and/or supplemental Fig. S1, the various sizes of IOMNs mainly accumulated in the liver and spleen, followed by lungs and kidney, and the least evidence of accumulation was observed in the stomach, intestine, and uterus at day 1 after injection. Surprisingly, the iron content was significantly lowest in the heart of mice treated with IOMNs compared with the control mice (the concentrations were 125.32±11.44 (10 nm), 113.69±5.97 (20 nm), 97.96±18.45 (30 nm), 104.22±16.87 (40 nm), and 177.08±50.07 μg/g (control), respectively as seen in Tab. 1). These data indicated that larger IOMNs caused a greater decrease in the iron content of the heart. The iron level in the brain were not significantly affected at day 1 post injection as shown in the Tab. 1 (18.14±2.33 (10 nm), 18.87±3.38 (20 nm), 18.07±4.40 (30 nm), 18.02±4.16 (40 nm), and 18.54±1.94 μg/g (control)). More interestingly, the smallest

IOMNs exhibited high uptake in the liver at day 1 post injection (the concentrations of various IOMNs were 540.93±169.14 (10 nm), 285.36±4.67 (20 nm), 313.09±29.24 (30 nm), 243.82±41.60 (40 nm), and 121.77±18.99 μg/g (control)), unlike the larger IOMNs that were more likely to have been trapped in the spleen (the largest concentration of iron (515.40±91.71μg/g)) as was observed in the group treated with 40 nm IOMNs. The high accumulation of the small IOMNs in liver were similar to published reports[14,28] using 5.2 nm and 10 nm NPs. The same observation for short-term uptake of large IOMNs in spleen had also been reported for QDs (4.5 nm) that were trapped in the spleen.[38]

At day 7 post injection, the levels of iron in the liver significantly decreased specifically for the 10 nm IOMNs. In contrast, iron contents in the spleen significantly increased except for the 40 nm IOMNs treatment group. It is possible that IOMNs degraded to release iron ions that entered into the metabolic process. This process, in turn, cleared the iron levels in the liver through iron binding proteins such as ferritin or transferrin (the store and transport systems for iron) that were mediated in liver endothelial and Kupffer cells.[22, 29] Iron contents in the spleen of animals treated with 10, 20, 30 nm IOMNs at longer time point (7 days) were increased (See Tab. 1 and supplemental Fig. S1b). It could be inferred based on previous reports[22] that these were a result of relatively higher expression of transferrin receptors and larger aggregates that were easily taken up by macrophages and B cells in the spleen. The distribution and transport behaviors of 10 nm IOMNs observed in the liver and spleen was highly consistent with a recent study involving 11±2 nm IOMNs.[22] It was

reported that NPs (InAs/ZnS and CdSe/ZnS QDs) with diameters less than 5.5 nm were easily and completely cleared from the kidney, whereas NPs with diameter > 15 nm were prevented from renal excretion.[28,30] Similar observations were confirmed in our study which showed that only 10 nm IOMNs were cleared from the kidney at day 7 post injection while the larger IOMNs (20, 30, and 40 nm) were not cleared; instead these were accumulated in the kidney (as shown in Tab. 1). At day 7 post injection, the iron contents in the brain were 26.92±6.19 (10 nm), 25.02±6.52 (20 nm), 20.59±2.75 (30 nm), 19.38±0.87 (40 nm), 18.69±0.56 μg/g (control) which showed a gradual increase with decrease in the size of the IOMNs. This suggested that the smaller IOMNs crossed the blood-brain barrier (BBB) at day 7 post injection. This was in agreement with the reports of Jain et al.[22] when they found that oleic acid-pluronic-coated iron oxide NPs were observed in the brain at 21 days post injection but not immediately after injection. Kim et al[25] and Wang et al.[5] also reported that iron oxide NPs (40 nm and 100 nm diameters) could penetrate the BBB without affecting the brain functions. Similarly, we did not observe any behavioral changes in the treated mice indicating that there were no significant effects on the central nervous system even when the iron levels increased. Only a small part of iron was transported to the brain in our study which could most probably be due to the early termination of the study at 7 days post injection. Accumulation of iron in the brain over extended treatment time could be a concern. Hence, in the future, longer time frame of observation need to considered.

Surprisingly, the iron contents in the heart of all treated groups were significantly decreased at both time points. In contrast, recent studies showed that the iron levels in the heart were increased following mice treatment with silica-coated IOMNs, oleic acid-pluronic-coated IOMNs, and Fe_3O_4 magnetic NPs.[5, 22, 25] This discrepancy in the iron levels in the heart may be due to the different sizes of iron oxide and the various surface coating properties, both of which can influence the IOMNs degradation and distribution. One possible consequence of our study could be the vital role of the heart in regulating the iron homeostasis *in vivo*. The low level of iron in the heart could most probably be a consequence of the iron binding to transferrin or other iron binding proteins that could lead to iron clearance from the heart (it could also be due to the low levels of expressed transferrin receptors). Elimination of IOMNs from mice was exhibited through the detection of iron in the animal feces that were detected at day 1, day 3 and day 7 post treatment; the percentage of iron excretion was not associated with the sizes of the IOMNs (as shown in Tab. 2 and/or supplemental Fig. S2). Previous studies had also shown slow clearance of iron over 7 weeks or 19 days after treatment with superparamagnetic iron oxide (AMI-25 or ferumoxtran-10),[33,39] which was in accordance with our findings, albeit done only over 7 days. Unfortunately, we did not monitor the iron content in blood, even though smaller IOMNs have a relative long half-life in blood. The high levels of iron in the liver, spleen, kidney, other organs, and feces in mice killed after day 7 post injections need further studies in the future.

Based on our data, the biodistribution, and transport of IOMNs over a short time frame post injection (7 days or less post injection) was a function of particle size that could be attributed to the levels of iron binding proteins such as haemosiderin, ferritin, and transferrin. Unfortunately, we did not monitor the levels of these proteins in the blood during our study, therefore, these parameters warrant close monitoring in future studies. A more extensive study taking various parameters that could shed light into the biodistribution and transport of IOMNs over a longer time frame will be considered for future studies.

Biochemistry and hematology results

NPs including IOMNs, metal, and metal oxides have similar sizes as those of viruses and large proteins which could easily induce inflammatory response, immune response, and could lead to a change in hematological parameters (like white blood cell count).[40,41] In our study, the IOMNs mainly showed accumulation in the liver, spleen, and kidney which were vital organs to investigate with or without induction of toxicity. Aside from observing the accumulation of IOMNs in these various organs, we also investigated for the presence of potential side effects on these organs as well as effects on their function by monitoring various serum biochemical markers that were indicators of liver and kidney functions such as alanine aminotransferase (ALT), aspartate aminotransferase (AST), total bilirubin (TBIL), direct bilirubin (DBIL), total protein (TP), albumin (ALB), globulin (GLB), the ratio of albumin to globulin (A/G), gamma glutamyl transaminase (GGT), alkaline phosphatase (ALP), creatinine (CRE),

blood urea nitrogen (BUN), and urea (UA). By monitoring the iron levels resulting from the degradation of IOMNs which could get incorporated with the hemoglobin of the red blood cells and the iron binding protein (transferrin) in a time-dependent manner,[22,39] we were able to evaluate the possible acute toxicity of the IOMNs in mice. The blood samples were harvested at day 1 and day 7 post IOMNs treatment (six mice were sacrificed per time point per group). As shown in Fig. 3, the seven important hepatic indicators (ALT, AST, TP, ALB, GLB, A/G, and GGT) were not significantly altered independent of the sizes of IOMNs treatment in comparison with the control. However, mice treated with the 10 nm IOMNs showed significantly increased levels of TBIL and DBIL; the ALP significantly decreased ($P<0.05$) but remained within the normal range on day 1 post injection. At day 7 post injection, all the results showed no significant difference in comparison with the control. The serum levels of TBIL, ALP, especially DBIL in 10 nm IOMNs treated group could be attributed to the observed high uptake of iron in the liver as shown on Tab. 1 which could have affected the excretion function of the bile duct. The monitored indicators of kidney function were CRE, BUN, and UA which exhibited similar levels as the control group. There were no significant variations observed among the various IOMNs treatment groups in both time points which could be associated with relatively low levels of iron in the kidney. In conclusion, there were no obvious hepatic and renal toxicity observed in the animals after IOMNs treatment, which suggested that the IOMNs studied were not toxic in vivo in mice.

NPs could be stored and degraded in the vasculature but the small IOMNs showed relatively longer half-life in blood.[19] IOMNs or component materials may interact with hematological factors such as red blood cells and white blood cells.[41] Therefore, we studied the following typical hematological indicators: white blood cells count (WBC), red blood cells count (RBC), hemoglobin (HB), polymorphomultinuclear neutrophil granulocyte (PMN), lymphocyte (LY), mean corpuscular hemoglobin concentration (MCHC), and platelet count (PLT). Representative hematological results listed in Fig. 4 did not significantly change except the WBC, PMN, and PLT in the IOMNs treatment groups compared with the control group. PLT showed a transient reduction on day 1 post injection which recovered to the same level as the control on day 7 post injection. Smaller IOMNs have been reported to show longer residence in the blood that may have significantly changed ($P<0.05$) the levels of WBC and PMN without causing significant toxicity. However, these changes could potentially affect the applications *in vivo* due to a higher number of 10 nm IOMNs that were phagocytosed and which were potentially eliminated by PMN. Since iron in the body is mostly found in hemoglobin[22] and IOMNs could be degraded and the released iron ions incorporated with hemoglobin in red blood cells in a time-dependent manner[39], the slight insignificant decrease in RBC and HB from the 10 nm IOMNs treatment group at day 7 post injection (Fig. 4b, c) may have resulted from the longer residence in blood that caused a disturbance in the iron homeostasis *in vivo*. However, the slight changes in the levels of the hematological indicators were

within the normal range[42] and did not manifest observable toxicity *in vivo*. Other hematological data were included in the supplemented Fig. S3.

Histology results

Further evaluation of IOMNs toxicity through histopathological examination of organs to determine potential tissue damage, inflammation, or lesions from exposure were performed. Three representative organs where iron significantly accumulated (the liver, spleen, and kidney) were used to prepare tissue slides that were fixed, stained, and analyzed. As shown in Fig. 5, no apparent histopathological abnormalities or lesions were observed in comparison with the control.

Gene expression changes in the liver

In order to investigate the subtle IOMNs induced changes *in vivo* (and it is known that inorganic NPs including IOMNs, titanium dioxide NPs, quantum dots easily induced oxidative stress, immune response, metabolic process change, apoptosis, and cell proliferation *in vitro* and *in vivo*[7,15,18-21,23,25,4351]) we followed the changes in gene expressions in the liver. We selected representative gene expression levels in the liver at day 7 post-injection. Heme oxygenase 1 (*Hmox1*) and glutamate-cysteine ligase catalytic subunit (*Gclc*) were considered the indicators of oxidative stress, and the nuclear factor erythroid 2 related factor 2 (*Nrf2*) has been used as a critical regulator of antioxidant response in biological systems in relevant studies.[43, 45] Furthermore,

Hmox1 protein was reported as a recognized biomarker in the CdSe/ZnS quantum dots induced cytotoxicity.[46] Several sensitive indictors of genes related to metabolic processes (Cytochrome P450, family 1, subfamily a, polypeptide 1, *Cyp1a1*; Proprotein convertase subtilisin/kexin type 9, *Pcsk9*; Acetyl-CoA acetyltransferase 2, *Acat2*), immune response (Interleukin 20, *IL20*; Trace amine-associated receptor 1, *Taar1*; Tumor necrosis factor receptor superfamily, member 11a, NFκB activator, *Tnfrsf11a*), apoptosis (*p53*; *Bcl2-bax*; V-fos FBJ murine osteosarcoma viral oncogene homolog, *Fos*), and cell proliferation (Leucine-rich repeat containing G protein-coupled receptor 4, *Lgr4*) were monitored.[44, 47-49] In addition, considering that the IOMNs could be degraded and may affect the expression of essential trace metal transporter genes, transferrin (*Trf*, a Fe transporter), metallothionein 1 (*Mt-1*, an inducible protein by metallic elements such as Cd), and Zrt- and Irt-related protein 14 (*Zip-14*, a Zn and Fe transporter) were also assessed.[45] As shown in Fig. 6, majority of the gene expressions including *p53*, *Zip-14*, *Pcsk9*, *Hmox1* and *Gclc* were all down-regulated in the animals that were exposed to IOMNs. *Pcsk9* and *Hmox1* showed the highest decrease in expression which declined over 130 times and 90 times, respectively from the treatment with all four sizes of IOMNs. This demonstrated that *Pcsk9* and *Hmox1* were extremely sensitive to exposure to IOMNs which could be indicative of minor oxidative stress and minor changes in metabolic processes but did not manifest toxicity in mice over the 7-day duration of this study. Thus, it is very important to follow the levels of these gene expressions in studies of longer or even extended duration in the future.

Only one gene, the *Nrf2* expression, was up-regulated among the animals that were exposed to four different sizes of IOMNs. Since the *Nrf2* has been used as a critical regulator of antioxidant response in biological systems as a cellular defense in the presence of oxidative stress, the up-regulation of its gene expression may be inferred as a response to IOMNs induced oxidative stress. Further studies following the gene expression of *Nrf2* in animal studies of longer or even extended duration in the future must be monitored.

Some gene expressions exhibited varying responses resulting from exposure to the four different sizes of IOMNs. For instance, the gene expression of *Taar1*, which is indicative of an immune response, increased in animals exposed to IOMNs that were less than 30 nm in diameter but decreased with the 40 nm IOMNs. In order to arrive at a conclusion for the *Taar1* expression behavior, we need further *in vivo* studies at extended periods.

Moreover, we attempted to explore if gene expression changes were dependent on the diameter of IOMNs following four sizes of IOMNs administration. Obviously, although the up-regulated and down-regulated of genes expression were observed, it was found that the smaller sizes of IOMNs (10 nm and 20 nm) showed more significant effects than the larger IOMNs (30 nm and 40 nm) for most of the genes. For instance, *Hmox1* expression level decreased with treatment from all the four sizes of IOMNs, while the 10 nm IOMNs induced the most significant decrease in gene expression (about -46.7150 times). Since Hmox1 is a rate-limiting enzyme in the degradation of heme to produce biliverdin, CO, and iron[43], it was possible that the

high concentration of iron in the liver of animals treated with 10 nm IOMNs may have suppressed the expression of *Hmox1*. It is necessary to perform *in vivo* studies over longer durations to verify the effects of 10 nm IOMNs on *Hmox1*.

The gene expression level evaluations demonstrated that even though no observable toxic effects were induced by the four sizes of IOMNs used in this study at 20 mg/kg over a 7-day duration, size related gene expression changes were found. These genes were specifically indicative of oxidative stress, immune response, iron transport, metabolic process, apoptosis, and more. However, it is imperative to perform *in vivo* studies over longer durations to further explore and/or confirm our observations.

Conclusion

We systematically explored the *in vivo* size dependent biodistribution, transportation, toxicity, and gene expression changes resulting from mice exposure to various sizes of carboxyl-coated IOMNs (10, 20, 30, 40 nm diameter). Data gathered indicated a size dependent biodistribution and gene expression changes (as shown in Fig. 7). The smallest IOMNs (10 nm) showed the highest uptake in the liver, whereas the largest IOMNs (40 nm) showed the highest uptake in the spleen on day 1-post injection. The 10 nm IOMNs was more easily cleared from the kidney and more readily penetrated the BBB. The 40 nm IOMNs was as readily accumulated as were cleared from the spleen. In addition, IOMNs did not show significant toxicity through analysis of blood biochemistry, and hematological plus histological assessment. However, the smaller IOMNs induced significant changes in the gene expression level of susceptible genes (such as *Pcsk9* and *Hmox1*) that were related to oxidative stress and metabolic processes. The potential adverse effects of IOMNs based on transcriptomics and proteomics *in vivo* must be performed to identify the biomarkers or key proteins and achieve conclusive results. Furthermore, long-term distribution, pharmacokinetics and toxicity and genotoxicity evaluation of IOMNs require further explorations to facilitate better understanding towards future applications of IOMNs in nanomedicine.

Acknowledgements

This work was supported by Training Plan for the Young Scientist (Jinggang Star) of Jiangxi Province (20142BCB23004), Major Program of Natural Science Foundation of Jiangxi Province, China (20143ACB21003), National Natural Science Foundation of China (81201691 and 31271863), the Innovation Special Fund Project for Graduate of Jiangxi Province in 2013 (YC2013-S050) and the Training Plan for the Main Subject of Academic Leaders of Jiangxi Province in 2009 and Ganpo Talent 555 Engineering Project. The authors would like to thank Dr. Andrew Wang and Dr. Hong Xu for providing valuable information and the materials of the IOMNs.

References

1 R. Qiao, C. Yang, M. Gao, *J. Mater. Chem.*, 2009, **19**, 6274-6293.

2 G. Liu, J. Gao, H. Ai, X. Chen, *Small*, 2013, **9**, 1533-1545.

3 H. Xu, Z. P. Aguilar, L. Yang, M. Kuang, H. Duan, Y. Xiong, H. Wei and A. Wang, *Biomaterials*, 2011, **32**, 9758-9765.

4 M. Muthiah , I. K. Park , C. S. Cho, *Biotechnol. Adv.*, 2013, **31**, 1224-1236.

5 J. Wang, Y. Chen, B. Chen, J. Ding, G. Xia, C. Gao, J. cheng, N. Jin, Y. Zhou, X. Li, M. Tang and X. M. Wang, *Int. J. Nanomed.*, 2010, **5**, 861-866.

6 D. Chen, Q. Tang, X. Li, X. Zhou, J. Zang, W. Xue, J. Xiang and C. Guo,. *Int. J .Nanomed.*, 2012, **7**, 4973-4982.

7 N. Singh, G. J. Jenkins, R. Asadi, S. H. Doak. *Nano Rev.*, 2010, **1**.

8 H. Lee, M. K. Yu, S. P. Park, S. Moon, J. J. Min, Y. Y. Jeong, H. W. Kang and S. Jon, *J. Am. Chem. Soc.*, 2007, **129**, 12739-12745.

9 Katsnelson B, Privalova LI, Kuzmin SV, Degtyareva TD, Sutunkova MP, O. S. Yeremenko, I. A. Minigalieva, E. P. Kireyeva, M. Y. Khodos, A. N. Kozitsina, N. A. Malakhova, J. A. Glazyrina, V. Y. Shur, E. I. Shishkin and E. V. Nikolaeva, *Int. J. Occup. Environ*. Health., 2010, **16**, 503-519.

10 Y. Pan, S. Neuss, A. Leifert, M. Fischler, F. Wen, U. Simon, G. Schmid, W. Brandau and W. Jahnen-Dechent, *Small*, 2007, **3**, 1941-1949.

11 H. L. Karlsson, J. Gustafsson, P. Cronholm, L. Möller, *Toxicol. Lett.*, 2009, **188**, 112-118.

12 E. K. Larsen, T. Nielsen, T. Wittenborn, H. Birkedal, T. Vorup-Jensen, M. H. Jakobsen, M. H. Jakobsen, L. Østergaard, M. R. Horsman, F. Besenbacher, K. A. Howard and J. Kjems, *Acs Nano*, 2009, **3**, 1947-1951.

13 A. R. Gliga, S. Skoglund, I. O. Wallinder, B. Fadeel and H. Karlsson, *Part. Fibre Toxicol.*, 2014, **11**, 11.

14 X. D. Zhang, D. Wu, X. Shen, P. X. Liu, N. Yang, B. Zhao, H. Zhang, Y. M. Sun, L. A. Zhang and F. Y. Fan, *Int. J. Nanomed.*, 2011, **6**, 2071-2081.

15 G. Sharma, V. Kodali, M. Gaffrey, W. Wang, K. R. Minard, N. J. Karin, J. G. Teeguarden and B. D. Thrall, *Nanotoxicology*. 2014, **8**, 663-675.

16 M. Mahmoudi, A. Simchi and M. Imani, *J. Phys. Chem. C*. 2009, **113**, 9573-9580.

17 D. B. Cochran, P. P. Wattamwar, R. Wydra, J. Z. Hilt, K. W. Anderson, R. E. Eitel and T. D. Dziubla, *Biomaterials*, 2013, **34**, 9615-9622.

18 M. Mahmoudi, A. Simchi, A. S. Milani and P. Stroeve. *J. Colloid. Interf. Sci.*, 2009, **336**, 510-518.

19 K. Muller, J. N. Skepper, M. Posfai, R. Trivedi, S. Howarth, C. Corot, E. Lancelot, P. W. Thompson, A. P. Brown and J. H. Gillard, *Biomaterials*. 2007, **28**, 1629-1642.

20 S. Naqvi, M. Samim, M. Abdin, F. J. Ahmed, A. Maitra, C. K. Prashant and A. K Dinda, *Int. J. Nanomed.,* 2010, **5**, 983-989.

21 Calero M, Gutiérrez L, Salas G, Luengo Y, Lázaro A, P. Acedo, M. P. Morales, R. Miranda and A. Villanueva, *Nanomed-Nanotechnol.*, 2014, **10**, 733-743.

22 T. K. Jain, M. K. Reddy, M. A. Morales, D. L. L. Pelecky and V. Labhasetwar, *Mol. Pharm.*, 2008, **5**, 316-327.

23 B. A. Chen, N. Jin, J. Wang, J. Ding, C. Gao, J. Cheng, G. Xia, F. Gao, Y. Zhou, Y. Chen, G. Zhou, X. Li, Y. Zhang, M. Tang and X. Wang, *Int. J. Nanomed.*, 2010, **5**, 593-599.

24 B. A. Katsnelson, T. D. Degtyareva, I. I. Minigalieva, L. I. Privalova, S. V. Kuzmin, O. S. Yeremenko, E. P. Kireyeva, M. P. Sutunkova, I. I. Valamina, M. Y. Khodos, A. N. Kozitsina, V. Y. Shur, V. A. Vazhenin, A. P. Potapov and M. V. Morozova, *Int. J. Toxicol.*, 2011, **30**, 59-68.

25 J. S. Kim, T. J. Yoon, K. N. Yu, B. G. Kim, S. J. Park, H. W. Kim, K. H. Lee, S. B. Park, J. K. Lee and M. H. Cho, *Toxicol. Sci.*, 2006, **89**, 338-347.

26 M. T. Zhu, W. Y. Feng, Y. Wang, B. Wang, M. Wang, H. Ouyang, Y. L. Zhao and Z. F. Chai, *Toxicol. Sci.*, 2009, **107**, 342-351.

27 A. Galeone, G. Vecchio, M. A. Malvindi, V. Brunetti, R. Cingolani and P. P. Pompa, *Nanoscale*, 2012, **4**, 6401.

28 H. S. Choi, B. I. Ipe, P. Misra, J. H. Lee, M. G. Bawendi and J. V. Frangioni, *Nano Lett.*, 2009, **9**, 2354-2359.

29 K. Briley-Saebo, A. Bjørnerud, D. Grant, H. Ahlstrom, T. Berg and G. M. Kindberg, *Cell Tissue Res.*, 2004, **316**, 315-323.

30 H. S. Choi, W. Liu, P. Misra, E. Tanaka, J. P. Zimmer, B. I. Ipe, M. G Bawendi and J. V Frangioni, *Nat. Biotechnol.*, 2007, **25**, 1165-1170.

31 O. A. Wong, R. J. Hansen, T. W. Ni, C. L. Heinecke, W. S. Compel, D. L. Gustafson and C. J. Ackerson, *Nanoscale*, 2013, **5**, 10525.

32 A. Ruiz, Y. Hernandez, C. Cabal, E. Gonzalez, S. Veintemillas-Verdaguer, E. Martınez and M. P. Morales, *Nanoscale*, 2013, **5**, 11400.

33 P. Bourrinet, H. H. Bengele, B. Bonnemain, A. Dencausse, J. M. Idee, P. M. Jacobs and J. M. Lewis, *Invest Radiol.*, 2006, **41**, 313-324.

34 L. Yang, H. Mao, Y. A. Wang, Z. Cao, X. Peng, X. Wang, H. Duan, C. Ni, Q. Yuan, G. Adams, M. Q. Smith, W. C. Wood, X. Gao and S. Nie, *small*, 2009, 5, 235-243.

35 K. J. Livak and T. D. Schmittgen, *Methods*, 2001, **25**, 402-408.

36 A. A. Romoser, P. L. Chen, J. M. Berg, C. Seabury, I. Ivanov, M. F. Criscitiello and C. M. Sayes, *Mol. Immunol.*, 2011, **48**, 1349-1359.

37 Y. Zhao, Q. Wu, Y. Li, A. Nouara, R. Jia and D. Wang, *Nanoscale*, 2014, **6**, 4275.

38 Y. Su, F. Peng, Z. Jiang, Y. Zhong, Y. Lu, X. Jiang, Q. Huang, C. Fan, S.T. Lee and Y. He, *Biomaterials*, 2011, **32**, 5855-5862.

39 R. Weissleder, D. Stark, B. Engelstad, B. Bacon, C. Compton, D. White, P. Jacobs and J. Lewis, *Am. J. Roentgenol.*, 1989, **152**, 167-173.

40 A, Nel, T. Xia, L. Mädler and N. Li, *Science*, 2006, **311**, 622-627.

41 T. S. Hauck, R. E. Anderson, H. C. Fischer, S. Newbigging and W. C. W. Chan, *Small*, 2010, **6**, 138.

42 J. Liu, F. Erogbogbo, K. T. Yong, L. Ye, J. Liu, R. Hu, H. Chen, Y. Hu, Y. Yang and J. Yang, *ACS Nano*, 2013, **7**, 7303-7310.

43 Q. Sun, D. Tan, Q. Zhou, X. Liu, Z. Cheng, G. Liu, M. Zhu, X. Sang, S. Gui, J. Cheng, R. Hu, M. Tang and F. Hong, *J. Biomed. Mater. Res. Part. A*, 2012; **100A**, 2554–2562.

44 S. Gui, Z. Zhang, L. Zheng, Y. Cui, X. Liu, N. Li, X. Sang, Q. Sun, G. Gaoa, Z. Cheng, J. Cheng, L. Wang, M. Tang and F. Hong, *J. Hazard Mater.*, 2011, **195**, 365–370.

45 C. H. Lin, M. H. Yang, L. W. Chang, C. S. Yang, H. Chang, W. H. Chang, M. H. Tsai, C. J. Wang and P. Lin, *Nanotoxicology*, 2011, **5**, 650 – 663.

46 L. A. McConnachie, C. C. White, D. Botta, M. E. Zadworny, D. P. Cox, R. P. Beyer, X. Hu, D. L. Eaton, X. Gao and T. J. Kavanagh, *Nanotoxicology*, 2012, 1– 11.

47 X. Sang, L. Zheng, Q. Sun, N. Li, Y. Cui, R. Hu, G. Gao, Z. Cheng, J. Cheng, S. Gui, H. Liu, Z. Zhang and F. Hong, *J. Biomed. Mater. Res. Part. A*, 2012, **100A**, 894–902.

48 Y. Cui, Z. Zhang, H. Liu, Y. Ze, Y. Hu, Z. Cheng, J. Cheng, R. Hu, G. Gao, L. Wang, M. Tang and F. Hong, *Toxicol. Sci.*, 2012, **128**,171-185.

49 S. K. Balasubramanian, J. Jittiwat, J. Manikandan, C. N. Ong, L. E. Yu and W. Y. Ong, *Biomaterials*. 2010, **31**, 2034–2042.

50 Q. Wu, Y. Zhao, J. Fang and D. Wang, *Nanoscale*, 2014, **6**, 5894.

51 V. Brunetti, H. Chibli, R. Fiammengo, A. Galeone, M. A. Malvindi, G. Vecchio, R. Cingolani, J. L. Nadeau and P. P. Pompa, *Nanoscale*, 2013, **5**, 307.

Figure captions

Figure. 1 Characterizations of carboxyl coated iron oxide magnetic nanoparticles (TEM and DLS). a-d) are showed the diameters of four sizes of IOMNs: the 10 nm IOMNs (a), 20 nm IOMNs (b), 30 nm IOMNs (c), and 40 nm IOMNs (d). Scale bar: 100 nm. e) represent the hydrodynamic sizes and zeta potentials of various IOMNs, n=4.

Figure. 2 Body weight of Kunming mice following intravenous injection of various sizes of IOMNs. All the administration doses were 3 mg/mL×100 μL×2. These represent the mean and standard deviation, n=6.

Figure. 3 Serum biochemical analysis from animals treated with various sizes of IOMNs and control. a-m) results represent the mean and standard deviation of ALT (a), AST (b), TBIL (c), DBIL (d), TP (e), ALB (f), GLB (g), A/G (h), GGT (i), ALP (j), CRE (k), BUN (l), and UA (m). Abbreviations: alanine aminotransferase, ALT; aspartate aminotransferase, AST; total bilirubin, DBIL; direct bilirubin, DBIL; total protein, TP; albumin, ALB; globulin, GLB; the ratio of albumin to globulin, A/G; gamma glutamyl transaminase, GGT; alkaline phosphatase, ALP; creatinine, CRE; blood urea nitrogen, BUN; and urea, UA, n=6. *: $P < 0.05$ versus the control group.

Figure. 4 Whole blood analysis from animals treated with various sizes of IOMNs and control. a-j) results represent the mean and standard deviation of white blood cells count, WBC (a); red blood cells count, RBC (b); hemoglobin, HB (c); neutrophil granulocyte, NE (d), lymphocyte, LY (e), mean corpuscular hemoglobin concentration,

MCHC (f), and platelet count, PLT (j), n=6. *: $P < 0.05$ versus the control group.

Figure. 5 Histological images in treated animals exhibit no signs of toxicity. Liver, spleen, and kidney from animals treated with various sizes of IOMNs and control. D1 and D7 mean the organs were collected from mice on day 1 and day 7 post injections, n=6.

Figure. 6 Size related gene expression changes of various sizes of IOMNs in liver at 7 d post injection. The relative expression ratio was presented as a $\log_2$ value in the histogram. A ratio greater than zero indicated up-regulation of gene expression, whereas a ratio below zero indicated down-regulation.

Figure. 7 The proposed size dependent biodistribution and gene expression changes resulting from treatment with of various sizes of IOMNs based on the data accumulated in this study. D1, D3, and D7 mean the organs or tissues were collected from mice post-injection in day 1 and day 7, n=6.

Figures

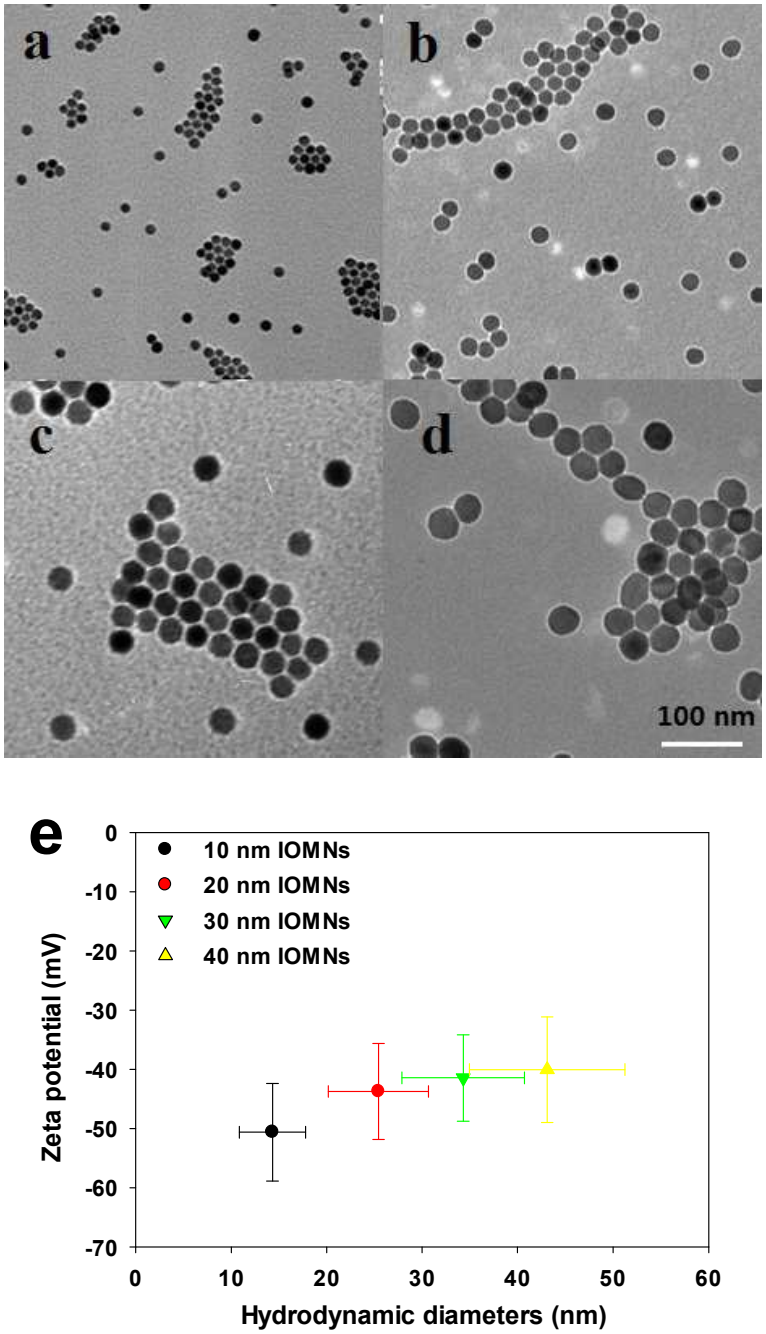

Fig.1. Yang *et al.*

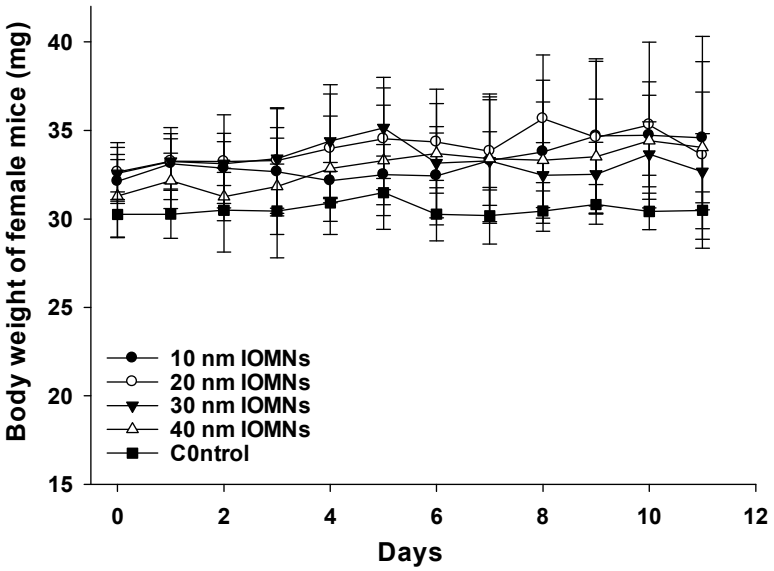

Fig. 2. Yang *et al*.

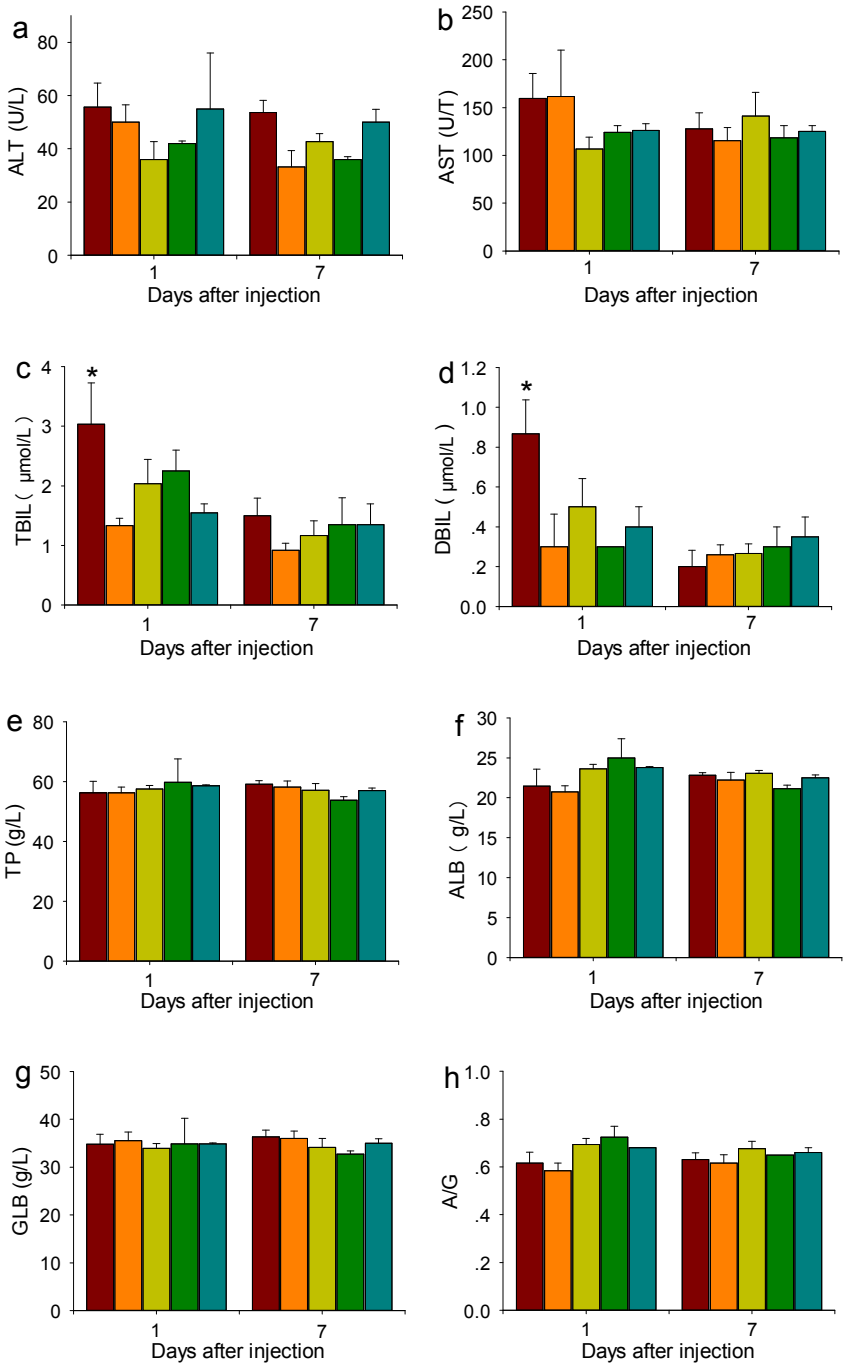

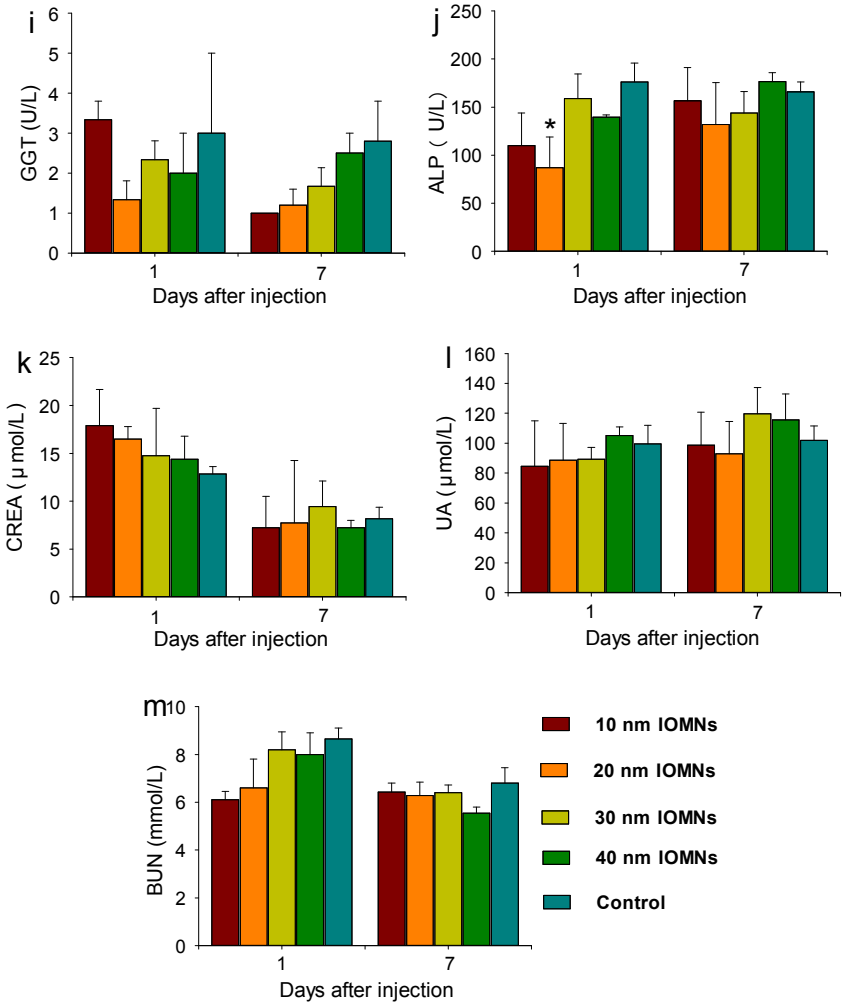

Fig. 3. Yang *et al*.

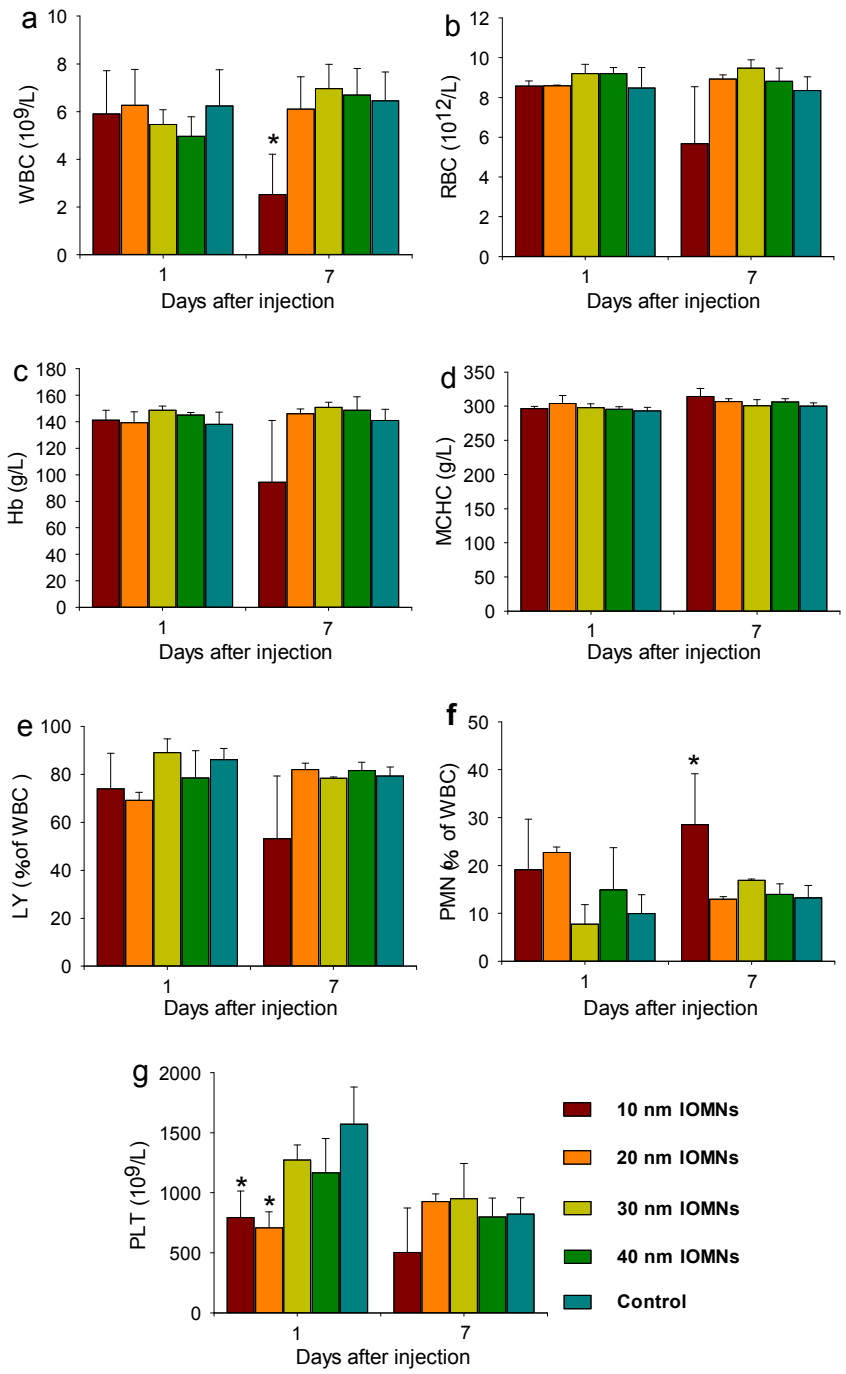

Fig. 4. Yang *et al.*

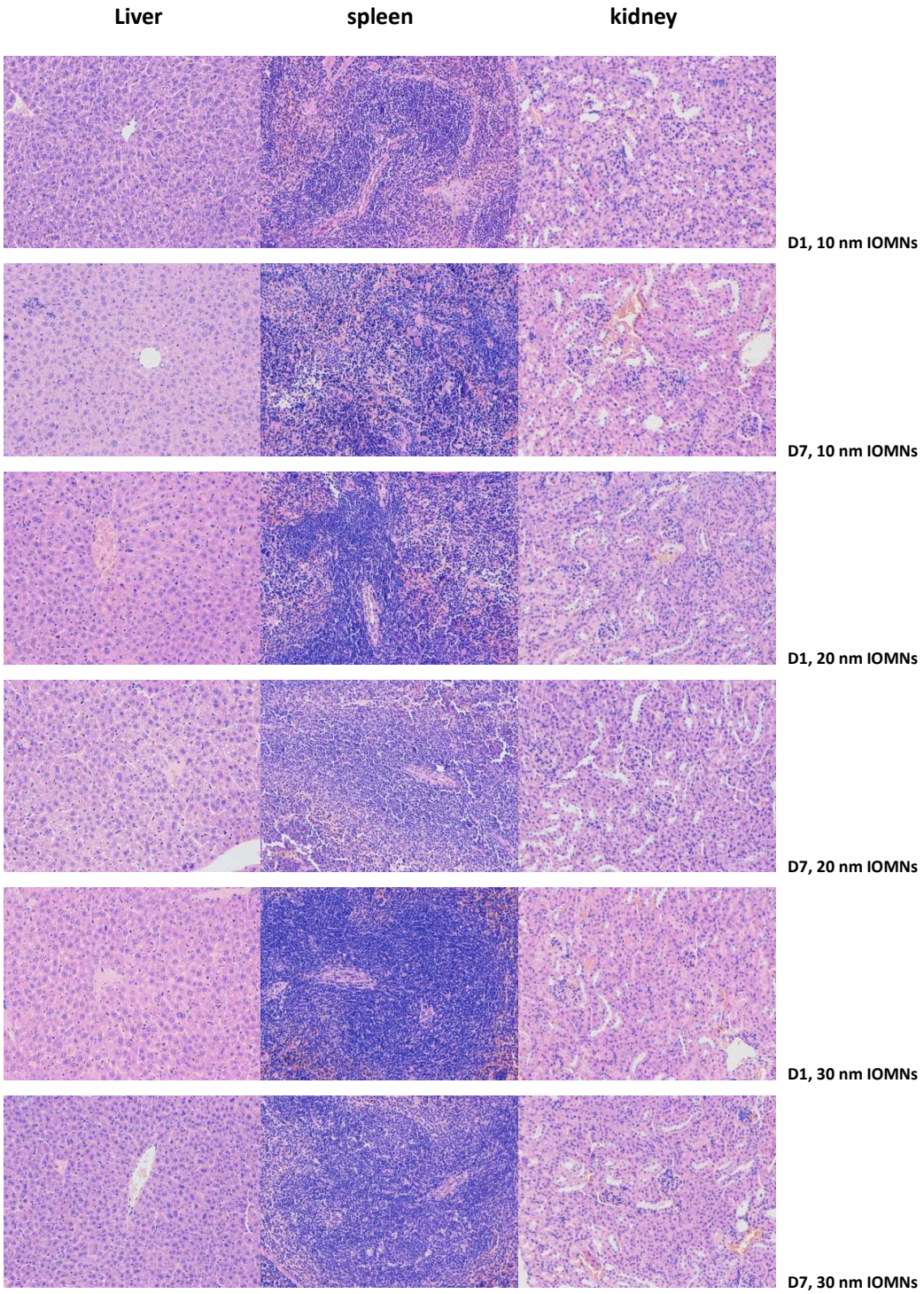

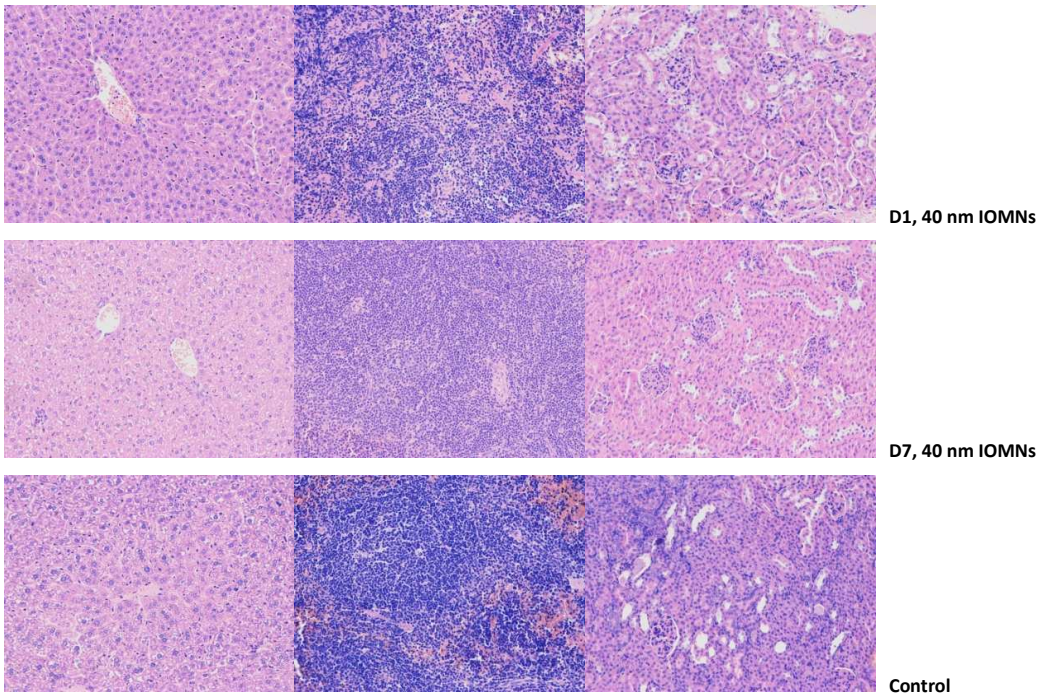

Fig. 5. Yang *et al*.

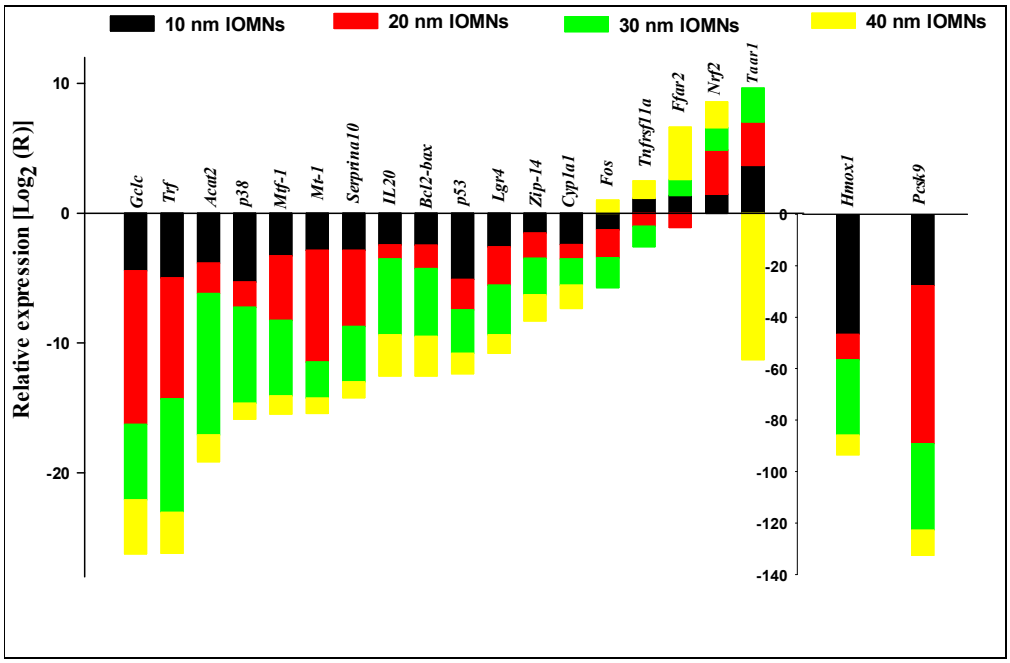

Fig. 6. Yang *et al*.

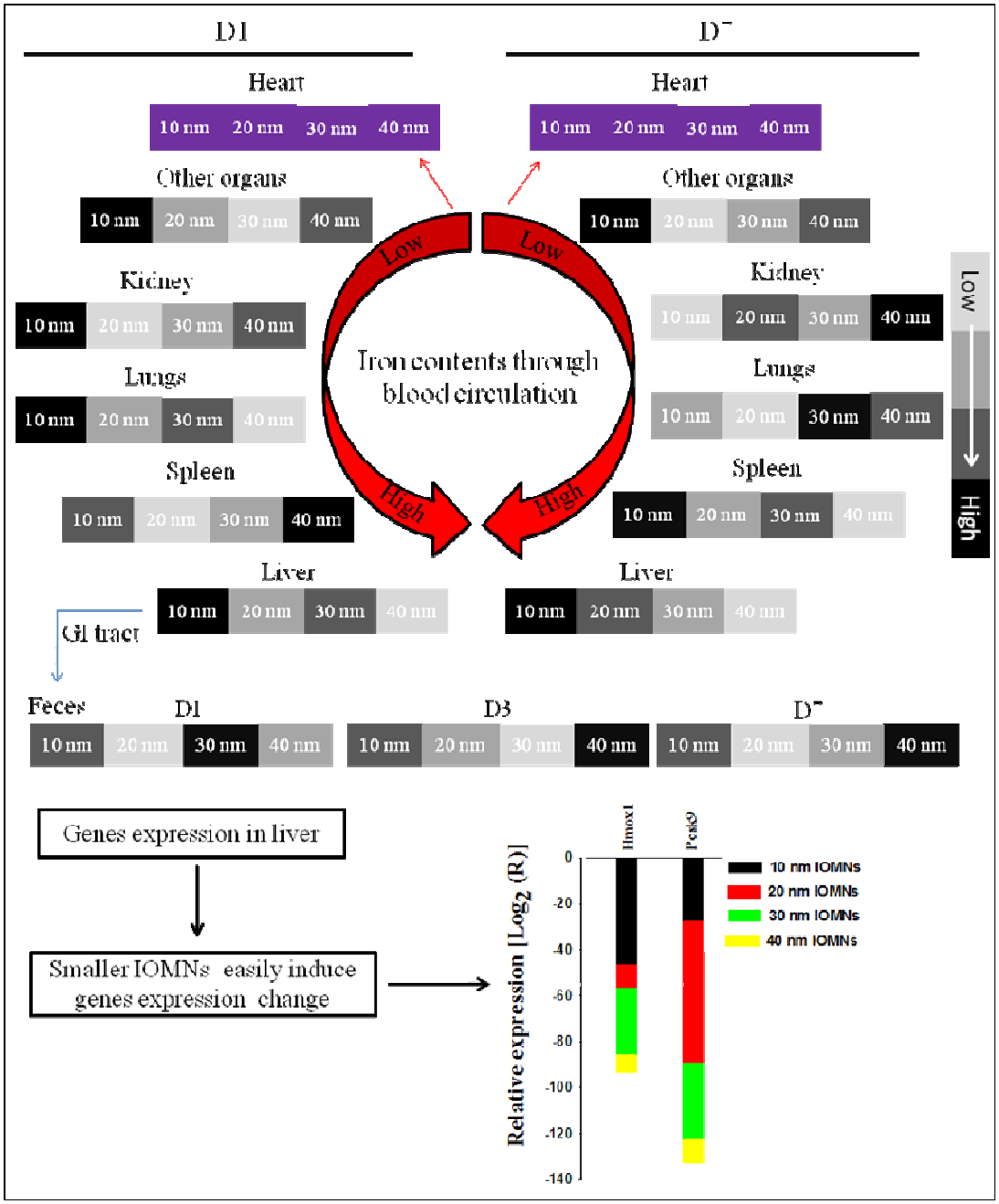

Fig. 7. Yang *et al*.

Tables

Table 1. Size dependent biodistribution of various sizes of IOMNs at 1 d (A) and 7 d (B) after injection. These results show mean and standard deviation of iron contents in these organs at both time points. D1 and D7 mean the organs were collected from mice post-injection in day 1 and day 7, n=6. *: P < 0.05 versus the control group; **p<0.01 versus the control group.

IOMNs	Heart (μg/g)	Liver (μg/g)	Spleen (μg/g)	Lung (μg/g)	Kidney (μg/g)	Brain (μg/g)	Stomach (μg/g)	Intestine (μg/g)	Uterus (μg/g)
10 nm (D1)	125.31± 11.48*	540.93±169.13**	358.83±40.47*	169.40±9.99*	93.41±5.41**	18.14±2.13	55.72±15.18**	46.62±7.98**	37.22±7.11
20 nm (D1)	113.70 ± 5.97**	285.36 ± 4.68*	252.67±38.57	143.71±20.40	82.79±5.66**	18.87±3.39	30.44±8.52	40.19±7.02	30.96±7.28
30 nm (D1)	97.97 ± 18.45**	313.09±29.24**	325.57±30.71**	168.42±8.21*	85.61±3.14**	18.07±4.40	34.28±2.56	31.75±9.38**	26.73±3.27
40 nm (D1)	104.22±16.87**	243.83±41.61*	515.39±91.71	159.20±30.48*	88.09±11.66**	18.02±4.17	43.20±4.36	47.50±12.74	36.05±16.83
Control (D1)	177.08±50.07	121.77±18.99	277.63±6.01	117.45±44.93	62.57±11.02	18.54±1.94	36.93±1.89	27.74±0.49	28.87±3.37
10 nm (D7)	115.84±12.56*	369.79±42.17**	506.26±102.73**	139.08±19.32	79.81±3.44*	26.92±6.19*	56.93±2.83*	40.08±3.85*	36.67±6.30
20 nm (D7)	125.25±42.86*	281.82±49.72**	373.94±11.72	125.59±15.81	97.78±11.91**	25.03±6.52	44.43±3.60	32.05±7.13	30.03±5.35
30 nm (D7)	137.28±22.94	268.62±27.13**	467.44±132.11**	195.58±41.50*	93.68±10.35**	20.59±2.75	60.04±19.74*	35.09±16.28*	26.06±3.30
40 nm (D7)	121.59±14.37*	181.56±23.09*	394.88±51.12	152.98±25.01	98.65±13.81**	19.38±0.86	57.74±0.22*	40.01±0.24*	30.30±6.66
Control (D7)	181.49±49.29	112.96±7.07	279.05±7.79	129.75±35.93	63.37±8.10	18.69±0.57	38.17±1.19	28.31±0.61	30.16±2.34

Table 2. Iron levels in animal feces as indicator of IOMNs elimination at serial time points post injection. These results show mean and standard deviation, D1, D3, and D7 mean the organs were collected from mice post-injection in day 1, day 3, and day 7, respectively. n=6. *: $P < 0.05$ versus the control group.

Day	Feces samples (μg/g)				
	10 nm IOMNs	20 nm IOMNs	30 nm IOMNs	40 nm IOMNs	Control
D1	182.05± 39.80*	158.25± 24.01	183.02± 5.64*	180.33± 14.87*	132.02± 11.17
D3	189.55± 23.01*	187.76± 28.89*	159.17± 18.32	201.10± 11.74*	127.74± 7.29
D7	194.37± 29.84*	173.52± 6.50	186.50± 13.22*	197.72± 59.39*	132.52± 6.67

Graphical abstract

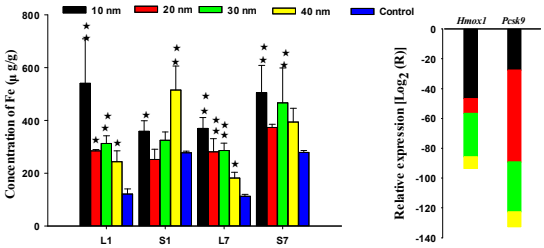

Size dependent biodistribution and gene expression changes of various IOMNs *in vivo*